

Article

The Change in Dynamic Response Distribution of Double-Track Tunnel Structure Caused by Adding Middle Partition Wall

Shuguang Yao^{1,2,3}, Jiani He^{1,2,3} and Ping Xu^{1,2,3,*}

¹ Key Laboratory of Traffic Safety on Track, Central South University, Ministry of Education, Changsha 410075, China

² Joint International Research Laboratory of Key Technology for Rail Traffic Safety, Central South University, Changsha 410075, China

³ National & Local Joint Engineering Research Center of Safety Technology for Rail Vehicle, Central South University, Changsha 410075, China

* Correspondence: xuping@csu.edu.cn

Abstract: Adding a middle partition wall is an effective method to prevent the interaction between the upper and lower subway lines in a double-track tunnel, and the subsequent change in the dynamic response of the tunnel structure caused by adding a middle partition wall has drawn attention. We analyzed the displacement and acceleration responses of the upper part (zone A), the lower part (zone B), the tunnel bed and the surrounding connecting part (zone C) of the double-track tunnel by establishing a two-dimensional finite element model of the double-track tunnel and soil with and without a middle partition wall. The numerical results demonstrate that the addition of the middle partition wall improves the displacement and acceleration response distribution of the double-track tunnel structure. Compared with single-train traffic, the addition of the middle partition wall brings more obvious changes to the dynamic response of the double-track tunnel during double-train traffic. The maximum displacement response decreases from 5.881 mm to 5.335 mm, and the maximum acceleration response decreases from 18.51 m/s² to 16.62 m/s². The displacement response value in the upper part increases from 1.0 mm to 1.5 mm, the acceleration response value increases from 3.0 m/s² to 4.6 m/s², the displacement response value in the tunnel bed and the surrounding connecting part decreases from 5.0 mm to 3.0 mm, and the acceleration response value in the tunnel bed and the surrounding connecting part decreases from 18.0 m/s² to 10.0 m/s². There is no obvious change in the lower part. During double-train traffic, after adding the middle partition wall, the horizontal displacement and horizontal acceleration response values of the double-track tunnel structure decrease by about 30% to 45%; the vertical displacement response value of the connection between the middle partition wall and the lining increases from 1.337 mm to 1.774 mm, an increase of 32.7%, and the vertical acceleration of the lower half of the tunnel lining is partially transferred to the upper half. The response values of horizontal displacement and acceleration in the middle part of the middle partition wall are the largest, at 1.6 mm and 6.0 m/s², while the response values of vertical displacement and acceleration in the bottom of the partition wall are the largest, at 3.3 mm and 9.0 m/s². The research results provide a reference for the structural design of middle partition walls to ensure the safety and stability of trains running in double-track tunnels.

Keywords: double-track tunnel; dynamic response; middle partition wall; numerical simulation



Citation: Yao, S.; He, J.; Xu, P. The Change in Dynamic Response Distribution of Double-Track Tunnel Structure Caused by Adding Middle Partition Wall. *Buildings* **2022**, *12*, 1711. <https://doi.org/10.3390/buildings12101711>

Academic Editors: Qi Zhang, Guozhu Zhang and Xiaobin Ding

Received: 31 August 2022

Accepted: 13 October 2022

Published: 17 October 2022

Publisher's Note: MDPI stays neutral with regard to jurisdictional claims in published maps and institutional affiliations.



Copyright: © 2022 by the authors. Licensee MDPI, Basel, Switzerland. This article is an open access article distributed under the terms and conditions of the Creative Commons Attribution (CC BY) license (<https://creativecommons.org/licenses/by/4.0/>).

1. Introduction

With the substantial increase in the speed of urban rail transit, and in order to satisfy the higher requirements of passengers for comfort, large-section double-track tunnels have become a development trend. However, when accidents such as collisions and fires occur in a double-track tunnel, they easily interfere with the operation of trains on

another track, resulting in more serious accident consequences and losses. For example, on 18 August 1991, a fire broke out in the Dayaoshan tunnel. Passengers jumped out of the train to escape and were in a dangerous position between the upper and lower subway lines. At this time, a freight train entered the tunnel and collided with some other vehicles. Among the passengers who escaped through the windows, 10 people died on the spot, 16 people were seriously wounded, and 4 people were slightly injured, which constituted a major casualty accident of the passenger train. Therefore, the addition of a middle partition wall in a double-track tunnel has become an effective method to mitigate such accidents, and the impact of the addition of a middle partition wall on the dynamic response of the double-track tunnel under the train vibration load and the dynamic response law of the middle partition wall structure must be investigated to ensure tunnel structure stability and safe train operation.

At present, many scholars have conducted in-depth research on the dynamic response of the double-track tunnel structure under the vibration load of a train from four aspects: physical model test, on-site measurement, theoretical prediction, and numerical simulation. Wya et al. experimentally studied the effect of cross-sectional shape on the dynamic response of the tunnel, and tested circular, rectangular, and horseshoe-shaped tunnel models [1]. Through dynamic centrifuge tests and numerical analysis, Tsinidis analyzed the significant effects of lining stiffness and soil–tunnel interface characteristics on dynamic lining stress [2]. Dmz et al. used centrifuge tests and numerical simulation methods to study the mechanical behavior of large-diameter shield tunnels, and proposed design suggestions for multi-layer formation large-diameter shield tunnels [3]. Li et al. conducted large-scale geomechanical model tests and numerical simulations, revealing the destructive behavior of the lining structure of the extra-large section tunnel, and the results showed that the strength of the lining structure in the tunnel vault and other parts should be strengthened [4]. Fan et al. used theoretical analysis methods to predict the dynamic response of the ring lining tunnel with imperfect interface, and derived the stress and displacement expressions of rock mass and lining based on the wave function expansion method and the linear spring model [5]. Huang et al. established a damage constitutive model, calculated and analyzed the dynamic response of a typical high-speed rail tunnel structure, and found that the maximum damage was concentrated on the near-earth side of the lower arch under the rail [6]. Real et al. constructed two-dimensional and three-dimensional finite element models of railway tunnels, and found that the results of the three-dimensional finite element model were relatively accurate, but the calculation time was longer and the calculation demand was large [7]. Luo et al. studied the mechanical behavior of long-span three-arch tunnel lining, and the results provided a reference for the design and construction of long-span three-arch tunnels [8]. Based on the actual situation of the large-diameter shield tunnel project of the main trunk canal of the Zhengzhou Intercity Railway, Gao Yu et al. used the plane strain model to simulate and analyze the change law of the vibration response of the tunnel train under the influence of factors such as the speed and tunnel burial depth of the single and double trains, and clarified the sensitive characteristics of different influencing factors to the vibration response of the tunnel, which provided a design reference and basis for the selection of the tunnel line [9]. Based on the first practice of intercity railway double-track large-diameter shield tunnel engineering, Li et al. established a two-dimensional finite element model and considered the influence of track unevenness value, waveform wear, and other factors, and studied the dynamic response law of tunnel lining when the train running speed was 200 km/h, and the results showed that the impact of double-train traffic and track unevenness on tunnel lining stress was greater [10]. Bai et al. established a two-dimensional finite element model of two close parallel tunnels, studied the elastoplastic dynamic response during single-train traffic and double-train traffic, and found that the dynamic response value during double-train traffic increased exponentially compared with that of single-train traffic [11]. The research objects in the described studies were railway tunnels without middle partition walls. There are not many studies on double-track tunnel with middle partition walls, and some scholars have

elaborated on the key construction techniques of middle partition walls in double-track tunnels [12–19]. Based on the engineering practice of the double-track large-section shield tunnel with a middle partition wall, Zhang et al. established a two-dimensional finite element model and studied the deformation characteristics of the double-track tunnel with a middle partition wall under different loads; the research results showed that the total vertical compression deformation of the middle partition tunnel is 2.8–2.9 mm under three kinds of loads [20]. Hu et al. used the display nonlinear finite element method to study the intersection condition of the double-track tunnel with a middle partition wall in Nanjing, and compared the vertical displacement of the node caused by the intersection of subway vehicles and the operation of a single train. The maximum displacement caused by the operation of a single train is 0.38 mm, and the maximum displacement caused by the intersection of subway vehicles is 0.6 mm. The results showed that the displacement response is of small magnitude and the double-track tunnel is stable under the intersection condition [21].

According to the aforementioned literature, the existing research methods for tunnel dynamic response mainly include physical model tests, field measurements, theoretical predictions, and numerical simulations. At present, the research on improving the dynamic response of double-track tunnels is not deep enough, and adding the middle partition wall is an innovative method to improve the dynamic response of double-track tunnels. In this study, we established a double-track tunnel–soil 2D finite element model with and without a middle partition wall and calculated the time–history curve of the train vibration load at a running speed of 160 km/h. The dynamic response of the double-track tunnel caused by adding a middle partition wall is analyzed from two aspects of displacement response and acceleration response, and the dynamic response law of the middle partition wall structure itself is studied. The research results provide a reference for the structural design of middle partition walls to ensure the safety and stability of the trains running in double-track tunnels.

2. Finite Element Model

2.1. Structural Design of a Double-Track Tunnel with Middle Partition Wall

Based on the actual project of the rail transit airport connecting line tunnel, the diameter of the double-track tunnel of the middle partition wall is 13.6 m, the clearance area of the single-line tunnel is 45.87 m², and the left and right sides are the upper and lower subway lines, respectively. The main structures are the lining, inverted arch, the middle partition wall, ballast bed and rails, etc. The inner and outer diameters of the lining are 6.25 m and 6.80 m, respectively. The height of the middle partition wall is 9.136 m. Concrete and angle steel are used to connect the wall and the lining. The structure is shown in Figure 1.

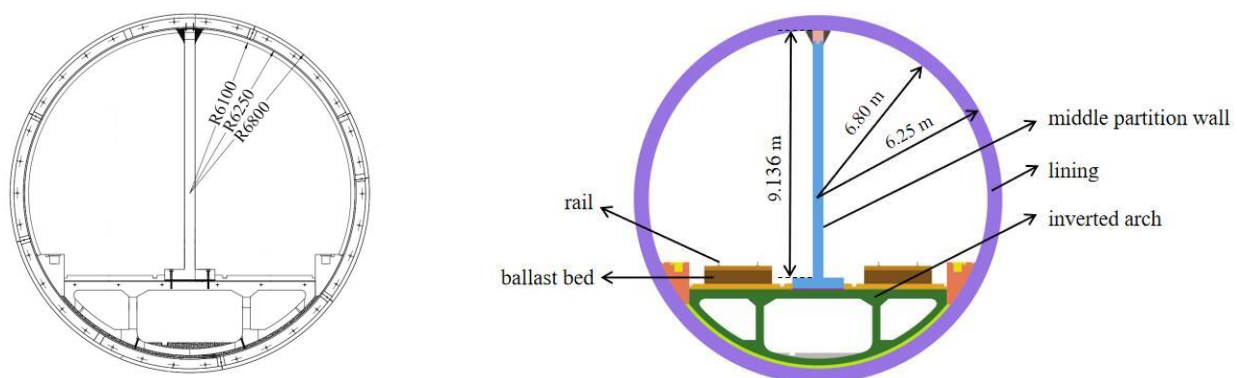


Figure 1. Section structure of double-track tunnel with middle partition wall.

2.2. Dynamics Fundamentals

Based on Hamilton's principle, when analyzing the dynamic response of the tunnel structure, the basic dynamic equation is as follows [22]:

$$[M]\{\ddot{\delta}\} + [C]\{\dot{\delta}\} + [K]\{\delta\} = [F(t)] \quad (1)$$

where $[M]$, $[C]$, and $[K]$ represent the mass matrix, damping matrix, and stiffness matrix, respectively. $[F(t)]$ represents the load of the structure. $\{\ddot{\delta}\}$, $\{\dot{\delta}\}$, and $\{\delta\}$ are the displacement, velocity, and acceleration vectors of the structure, respectively. The mass matrix, damping matrix, and stiffness matrix are calculated as follows:

$$[M_e] = \iiint \rho [N]^T [N] dV \quad (2)$$

$$[C_e] = \iiint c [N]^T [N] dV \quad (3)$$

$$[K_e] = \iiint [B]^T [D] [B] dV \quad (4)$$

where ρ is the material density, c is the material damping coefficient, $[N]$ is the shape function matrix, $[B]$ is the strain matrix, and $[D]$ is the node displacement matrix.

2.3. Establishment of Soil–Tunnel Finite Element Model

Using the finite element software RADIOSS, the three-dimensional problem of a several-kilometer-long tunnel is transformed into a two-dimensional plane strain problem for analysis and solution, and the tunnel cross-section is taken to establish a soil–tunnel model under the action of train vibration loads. PSHELL elements are used for soil and concrete. The mesh size of tunnel structures such as lining, inverted arch, and the partition wall is 100 mm [23]. Due to the large range of the soil layer, its mesh size can be slightly larger, which is taken as 500 mm in this paper.

In the numerical model, the interface elements between the soil and the tunnel structure are coupled. To ensure the correct interaction [24–26], there were no sliding or gap openings.

The elastoplastic model based on modern plastic theory is the most widely used model in geotechnical constitutive models. The Drucker–Prager model can be used to describe granular materials such as rock and soil. The Drucker–Prager model uses the Drucker–Prager yield criterion, which approximates Mohr–Coulomb to modify the Von Mises yield criterion. Both soil and concrete materials use the Drucker–Prager model in this paper [27–30], which is a simple modification of the Von Mises criterion, and its mathematical expression is:

$$F = \alpha J_1 + (J_2)^{0.5} - \kappa = 0 \quad (5)$$

where J_1 is the first invariant of stress and J_2 is the second invariant of stress. α and κ are the experimental constants related to the friction angle and adhesion force, respectively, inside the rock.

$$\begin{cases} \alpha = \frac{2 \sin \varphi}{\sqrt{3}(3 - \sin \varphi)} \\ \kappa = \frac{6C \cos \varphi}{\sqrt{3}(3 - \sin \varphi)} \end{cases} \quad (6)$$

where C is the cohesion and φ is the angle of internal friction.

As shown in Figure 2, the diameter of the tunnel is 13.6 m, and the lining thickness is 550 mm. According to the general design drawing of the double-track tunnel with the middle partition wall given by the cooperative enterprise, the minimum buried depth of the tunnel is 1D (13.6 m), and the soil layer from top to bottom comprises a silty clay layer (11.2 m), a powder clay layer (5.7 m), a fine silt layer (34.8 m), and a medium sand layer (5.5 m). In the general design drawing, the furthest measuring point required is 28 m, so

the left and right side and lower boundaries are taken 30 m from the outer side of the tunnel lining.

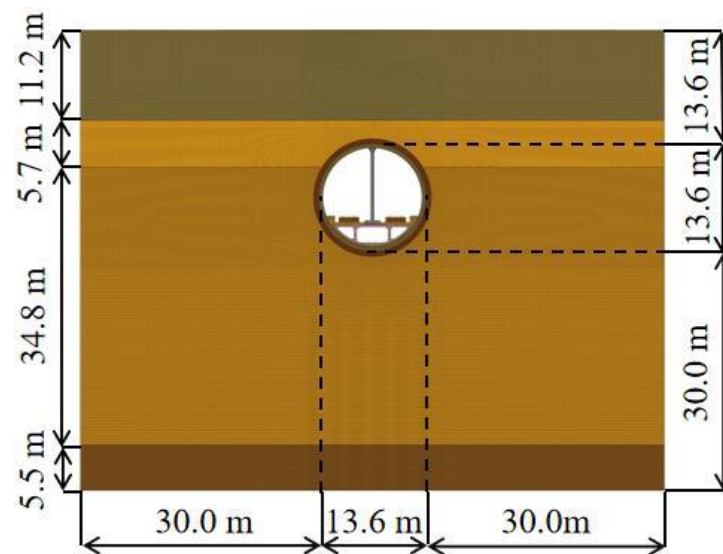


Figure 2. Soil–tunnel model.

2.4. Dynamic Boundary Conditions

In the field of geotechnical engineering, the soil in a certain range needs to be analyzed when the finite element method is used for simulation calculation. In order to achieve convergence, certain boundary conditions must be set. In dynamic analysis, if the vibration wave in the rock and soil is reflected when propagating to the boundary of the model, the reflected wave will be superimposed with vibration waves in the limited domain. The vibrations in actual soil spread outward, and the vibration wave superposition will strengthen the vibration response of soil in the finite field, which affects the accuracy of the calculation.

The viscous boundary was first proposed by Lysmer and Kuhlemeyer [31]. This method sets a damper at the boundary of the model to absorb the vibration wave, so that the vibration wave cannot be reflected indefinitely. It has high calculation accuracy and is a widely used boundary condition at present. As shown in Figure 3, the green grid cells are viscous artificial boundary cells. The dampers are set on the artificial boundary to absorb the energy transferred to the boundary, and the normal and tangential stresses are artificially applied along the boundary of the calculation area. Considering the geotechnical medium as a semi-infinite medium, the train vibration load is transferred from top to bottom, a viscous boundary is set, and viscous damping forces in two directions are applied along the boundary surface [32]:

$$\sigma_n = -\rho_0 C_p v_n \quad (7)$$

$$\sigma_s = -\rho_0 C_s v_s \quad (8)$$

where σ_n and σ_s are the normal and tangential stresses provided by the damper; ρ_0 is the boundary soil density; v_n and v_s are the boundary normal and tangential velocity components; and C_p and C_s are the incident compression wave and shear wave velocity, respectively. Among them, C_p and C_s are determined as follows:

$$C_p = \sqrt{\frac{K + 4G/3}{\rho_0}} \quad (9)$$

$$C_s = \sqrt{\frac{G}{\rho_0}} \quad (10)$$

where K and C are the bulk modulus and shear modulus of the soil, respectively.

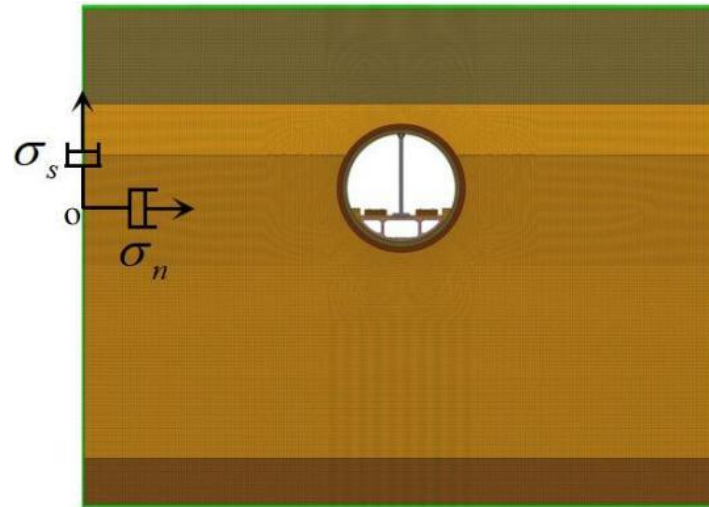


Figure 3. Schematic diagram of two-dimensional viscous artificial boundary.

2.5. Determination of Train Vibration Load

Li et al. found that the dynamic response of the tunnel structure under the train vibration load time–history curve obtained by three different methods has little difference—the structural dynamic stress and point displacement time–history curve are basically consistent [33]. In this paper, the excitation force function method [34–36], which is the most commonly used in research, is applied to simulate the train vibration load:

$$P(t) = k_1 k_2 (P_0 + P_1 \sin \omega_1 t + P_2 \sin \omega_2 t + P_3 \sin \omega_3 t) \quad (11)$$

where k_1 is the superposition coefficient of the adjacent wheel–rail force. According to the literature [37], the value of k_1 is generally 1.2–1.7, and is taken as 1.5 in this paper. k_2 is the dispersion coefficient of the rail, the value of k_2 is generally 0.6–0.9, taken as 0.7 in this paper. The unilateral static wheel weight is $P_0 = 80$ kN. P_1 , P_2 , and P_3 are the loads corresponding to a typical sag value in the control conditions I, II, and III in Table 1.

Table 1. Track geometry for uneven management of classical values.

Control Condition	Wavelength L_i (m)	Versine a_i (mm)
According to smooth driving (I)	50	16
	20	9
	10	5
According to the dynamic additional load acting on the line (II)	5	2.5
	2	0.6
	1	0.3
Wave wear (III)	0.5	0.1
	0.05	0.005

Let the unsprung mass of the train be M_0 , and the load amplitude is:

$$P_i = M_0 a_i \omega_i^2 \quad (12)$$

where ω_i is the circular frequency corresponding to I, II, and III conditions at the driving speed.

$$\omega_i = 2\pi v / L_i \quad (13)$$

where v is the running speed and L_i is the typical wavelength of the geometrically uneven curve.

Taking $M_0 = 750$ kg, $L_1 = 10$ m, $a_1 = 5$ mm; $L_2 = 1$ m, $a_2 = 0.3$ mm; and $L_3 = 0.5$ m, $a_3 = 0.1$ mm. Taking the train running speed $v = 160$ km/h, the total length of the six-series train is 140 m, and it takes 3.2 s to cross the tunnel section at a speed of 160 km/h. The time-history curve of the train vibration load is shown in Figure 4, which is applied vertically on the track tread.

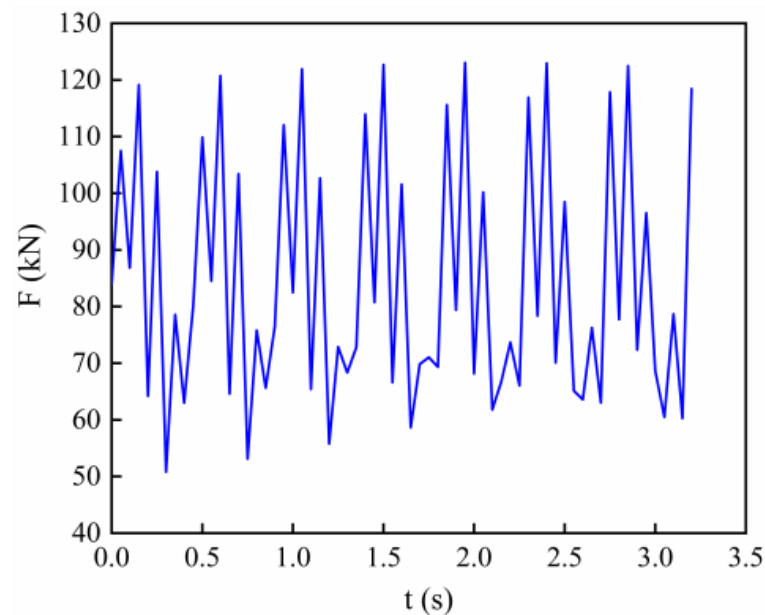


Figure 4. Vibration load time curve of train.

2.6. Soil Layer, Tunnel Material Parameters, and Damping

According to the *Technical Manual for Railway Engineering Design—Tunnel, the Second Design Institute of Ministry of Railways: Beijing, China* [38] and other relevant references [39], the specific values of the static material parameters of the main structures of each soil layer are shown in Table 2.

Table 2. Soil layer material parameters.

Material	Natural Density (kN/m ³)	Deformation Modulus (MPa)	Poisson Ratio	Cohesive Strength (kPa)	Internal Friction Angle (°)
Silt soil layer	16.8	2.0	0.41	11.0	7.1
Powder clay layer	18.3	4.0	0.35	17.0	11.5
Fine powder sand layer	19.3	20.0	0.28	0.0	30.0
Medium sand layer	19.8	25.0	0.31	0.0	32.0

The material of the tunnel lining and the track bed is C60 concrete, the material of an inverted arch and the middle partition wall is C40 concrete, the material of other concrete filling areas is C30 concrete, and the material of the rail is U71Mn. Usually, the cohesion of concrete is 300 kPa, and the internal friction angle is 60° [36]; it is safe to calculate according to these values. The specific values of the static material parameters of the core structure of the tunnel are shown in Table 3.

Table 3. Tunnel material parameters.

Material	Elastic Modulus (MPa)	Poisson Ratio	Density (kg/m ³)
C30	31,000	0.2	2500
C40	33,500	0.2	2500
C60	36,500	0.167	2400
U71Mn	206,000	0.3	7900

The material damping is Rayleigh damping [40]. The form of Rayleigh damping is composed of a mass matrix and a stiffness matrix:

$$[C] = \alpha[M] + \beta[K] \quad (14)$$

where $[C]$, $[M]$, and $[K]$ represent the damping matrix, mass matrix, stiffness matrix, respectively. α and β represent the mass damping and stiffness damping constant, respectively.

To obtain the desired formation results, a modal analysis of the model is performed with damping parameters α and β :

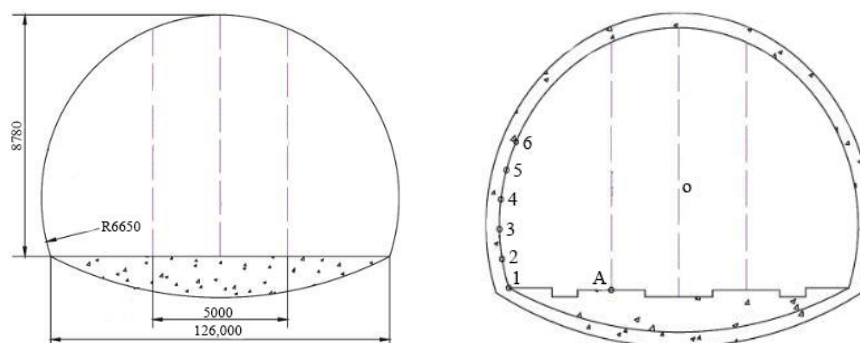
$$\alpha = \frac{2\omega_i\omega_j(\xi_i\omega_j - \xi_j\omega_i)}{\omega_j^2 - \omega_i^2} \quad (15)$$

$$\beta = \frac{2(\xi_j\omega_j - \xi_i\omega_i)}{\omega_j^2 - \omega_i^2} \quad (16)$$

The damping ratio ζ_0 of the soil layer around the tunnel is generally between 0.03 and 0.05, and the value in this paper is 0.05. From the above formula, the α of this model can be calculated as 0.533, and the β is 0.004.

3. Verification of Finite Element Model

In reference [41], the field test and numerical simulation analysis of a domestic high-speed railway double-track tunnel were carried out, and the transmission law of the dynamic acceleration response of the lining arch ring caused by a train passing through the tunnel at a speed of 300 km/h was analyzed. Figure 5 shows the tunnel contour and the location of the measuring points in the reference. The clear height of the tunnel is 8780 mm, the clear width is 126,000 mm, the inner diameter is 6650 mm, and the distance between the center line of the up and down line is 5000 mm. Taking the arch foot as the starting point, a measuring point is arranged every 1 m, with a total of six measuring points.

**Figure 5.** Tunnel contour and measuring point position.

In order to verify the accuracy of the calculation method in this paper, the material parameters, train vibration load, etc., in the reference are used as input parameters, and a numerical model is established according to the modeling method in this paper, as shown in Figure 6. In the model, the thickness of the soil layer on the left side and right side of the tunnel was set as 40 m, the thickness of the soil layer at the bottom was set as 40 m, and the

thickness of the soil layer at the top was set as 30 m. PSHELL elements were used for soil and concrete, and the mesh size of tunnel structures, such as lining, is 100 mm. Due to the larger range of the soil layer, its mesh size can be slightly larger, and is taken as 500 mm in this model. The material parameters of the model [41] are shown in Table 4. Figure 7 shows the load time–history curves of a train with a speed of 300 km/h.

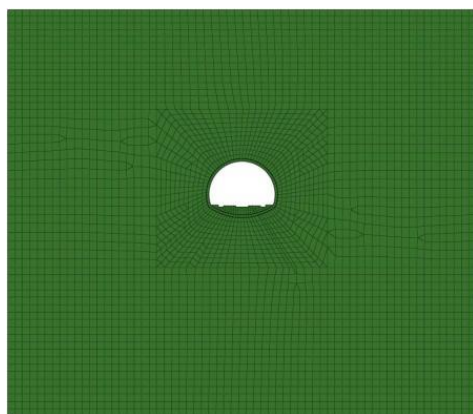


Figure 6. Numerical model.

Table 4. Main parameters of model material.

Material	Natural Density (kN/m ³)	Deformation Modulus (MPa)	Poisson Ratio	Cohesive Strength (MPa)	Internal Friction Angle (°)
IV level of surrounding rock	20	2.75	0.3	0.3	35
Primary support	21	24.6	0.21		
The secondary lining	25	31.4	0.2		

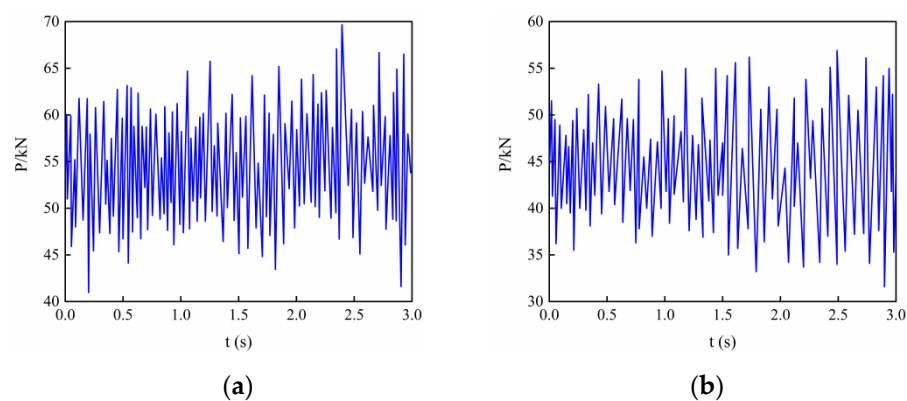


Figure 7. Vibration load time curve of train: (a) left side vertical force simulation value; (b) right side sag force simulation value.

When the train passes through the tunnel test section along the left line, the train is on the side close to the test point. Figure 8 shows the vertical and horizontal acceleration time–history curves of the reference and measuring point 6 in this paper, the black curve is obtained by the actual measurement, and the blue curve is calculated by the numerical model in this paper. It can be seen that the two acceleration trends are similar: the positive peak value of vertical acceleration is 2.264 m/s^2 , which appears at 0.74 s, and the negative peak value is -2.352 m/s^2 , which appears at 1.32 s; the positive peak value of horizontal acceleration is 2.125 m/s^2 , which appears at 1.63 s, the negative peak value of horizontal acceleration is -2.187 m/s^2 , which appears at 1.71 s. Compared with the acceleration time–

history curve, the two peaks are close, the peak time is close, and the error is within 5%. Therefore, the calculation method in this paper is accurate.

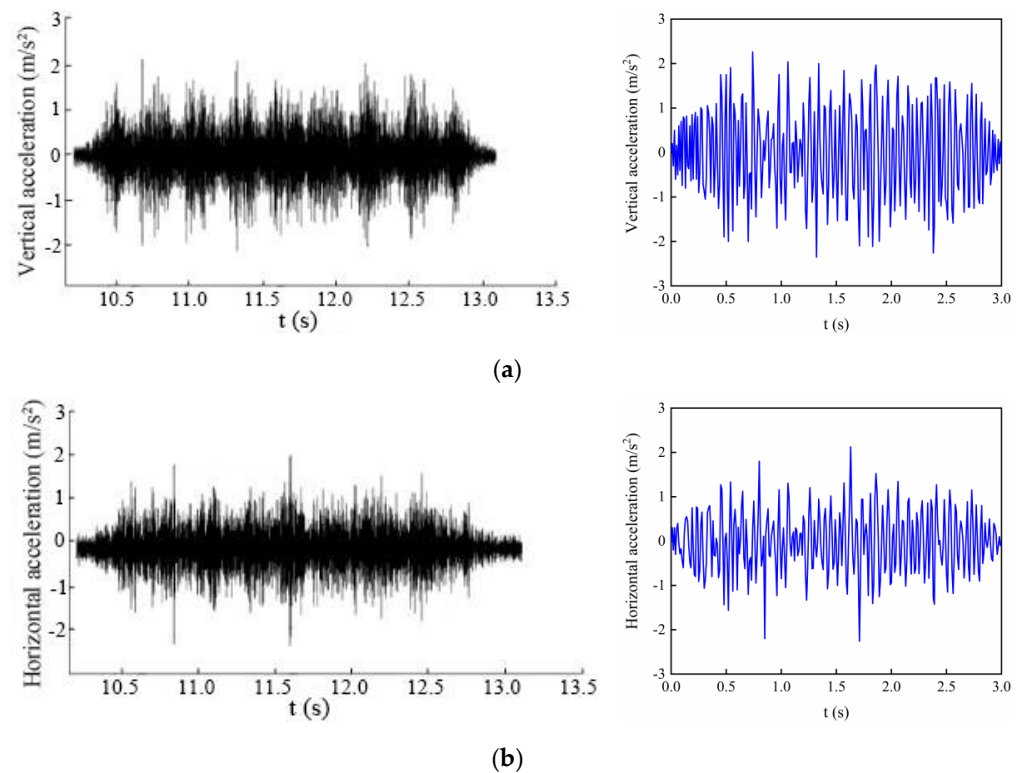


Figure 8. Measuring point acceleration time course curve: (a) vertical acceleration time–history curves of references and this paper; (b) the time–history curve of horizontal acceleration in the reference literature and this paper.

4. Results and Discussion

In order to obtain the change in the dynamic response of the tunnel structure under the train vibration load caused by the addition of the middle partition wall, the peak particle displacement (*PPD*) and the peak particle acceleration (*PPA*) of each measuring point in reference [42] are used as evaluation indicators in this paper. The calculation method of *PPD* is as follows:

$$PPD = |x(t)| \quad (17)$$

where t is the time, and $x(t)$ is the time–history curve of the displacement response of the model measuring point.

The calculation method of *PPA* is as follows:

$$PPA = |a(t)| \quad (18)$$

where t is the time, and $a(t)$ is the time–history curve of the acceleration response of the model measuring point.

As shown in Figure 9, a total of six measuring points (A1–A6) are arranged at the four end points of the double-track tunnel lining and at the positions of the arch feet, and six measuring points are arranged at the corresponding positions (B1–B6) of the double-track tunnel of the middle partition wall; the length of the partition wall is 9.136 m, the base is 0.4 m, and the measuring points are arranged on the part of the wall between the bottom of the groove at the top of the wall and the upper end face of the base, with a total length of 8.616 m. At the center line of the wall, there are five measuring points (C1–C5) evenly arranged from top to bottom.

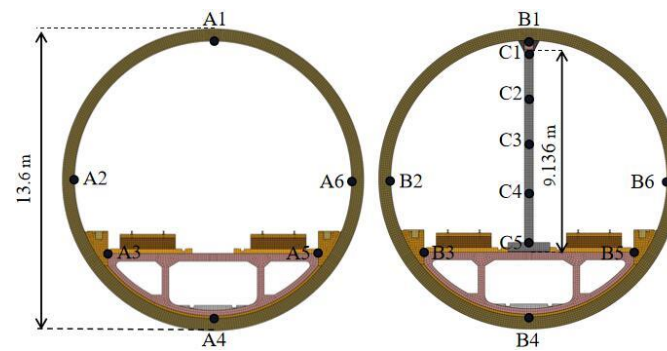


Figure 9. Tunnel model and measuring point location: A1–A6 are the measuring points on the lining and invert of the double-track tunnel; B1–B6 are the corresponding measuring points on the lining and invert of the double-track tunnel with the middle partition wall; C1–C5 are the measuring points on the middle partition wall.

4.1. Displacement Response Analysis

As shown in Figure 10, the tunnel structure is divided into three areas: the upper half of the tunnel (zone A), the lower half of the tunnel (zone B), and the track bed and surrounding connections (zone C). It can be found that at $t = 2.45$ s, the addition of the partition wall reduces the maximum displacement response value of the tunnel from 5.881 mm to 5.335 mm, and greatly weakens the displacement response of zone C, but the displacement response of zone A is slightly enhanced, while zone B has no significant change.

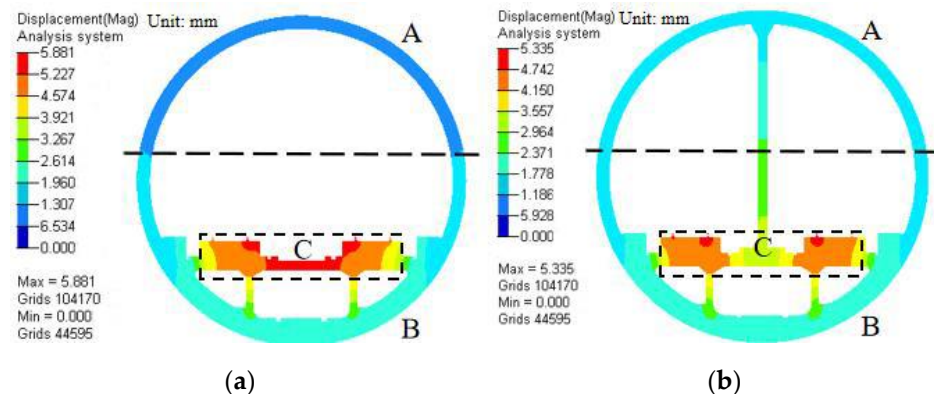


Figure 10. $t = 2.45$ s, tunnel displacement response during double-train traffic: (a) double-track tunnel; (b) double-track tunnel with middle partition wall; zone A is the upper half of the tunnel, zone B is the lower half of the tunnel, zone C is the track bed and surrounding connections.

During single-train traffic, the *PPHD* of A1–A5 is close to that of B1–B5. Comparing (a) and (b) in Figure 11, it can be clearly seen that A6 stands out, being 87.9% higher than the *PPHD* of B6. The *PPHD* itself is small, so the middle partition wall has little impact on it. The graph outlines of (c) and (d) in Figure 11 are similar, and the two are close, but the *PPVD* of B1 is 32.9% higher than that of A1. B1 is at the connection between the middle partition wall and the tunnel lining, and the train vibration load is applied in the form of vertical excitation load. The application of the middle partition wall makes the upper and lower parts of the tunnel lining have more connections, which transfers part of the vertical displacement response of the lower part to the upper part, so as to enhance the vertical displacement response of the joint. In general, during single-train traffic, the displacement response of the tunnel on one side of the train is greater than that on the other side. Except for the vertical displacement response of the double-track tunnel of the middle partition wall at the connection (B1) being slightly enhanced, the *PPVD* at the location is close to

that of the double-track tunnel; thus, the middle partition wall has little influence on the displacement response of the tunnel during single-train traffic.

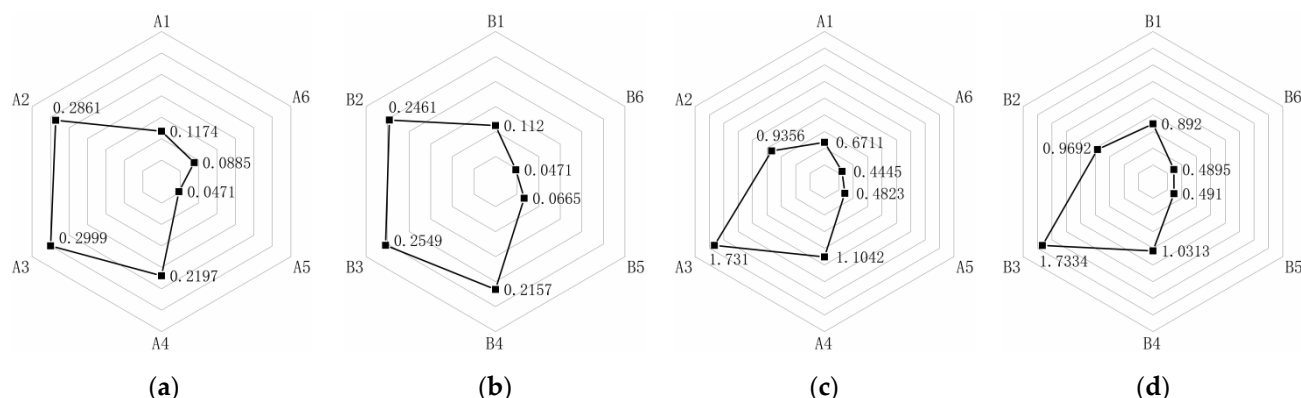


Figure 11. PPD (mm) during single-train traffic: (a) PPHD of double-track tunnel; (b) PPHD of double-track tunnel with middle partition wall; (c) PPVD of double-track tunnel; (d) PPVD of double-track tunnel with middle partition wall; A1-A6 and B1-B6 here correspond to that of A1-A6 and B1-B6 in Figure 9.

During double-train traffic, comparing (a) and (b) in Figure 12, it can be seen that their contours are consistent, bow-tie-shaped, and symmetrical on the left and right sides, and the PPHD at the axis of symmetry is the smallest. The PPHD is about 30% higher than that of the corresponding measuring points in the double-track tunnel of the middle partition wall. Although the outlines of graphs (c) and (d) in Figure 12 are symmetrical on both left and right sides, the PPVD of B1 is 32.7% higher than that of A1, protruding into a sharp corner shape. Except for A1 and B1, the PPVD of the rest of the measuring points is close. In general, during double-train traffic, the displacement responses of the double-track tunnel and the double-track tunnel with the middle partition wall are distributed symmetrically, but the horizontal displacement response of the double-track tunnel is stronger than that of the double-track tunnel with the middle partition wall. Similar to the vertical displacement response during single-train traffic, the application of the middle partition wall makes the upper and lower parts of the tunnel lining have more connections, which transfers part of the vertical displacement response of the lower part to the upper part, so as to enhance the vertical displacement response of the joint, and they grow at the same rate. The vertical displacement response values of the other measuring points are similar.

Hu Bao et al. [42] used the display nonlinear finite element method to study the intersection condition of the double-track tunnel with a middle partition wall in Nanjing, and compared the vertical displacement of the node caused by the intersection of subway vehicles and the operation of a single train. The maximum vertical displacement caused by the operation of a single train is 0.38 mm, and the maximum vertical displacement caused by the intersection of subway vehicles is 0.6 mm. The node position studied above corresponds to the B2 measuring point in this paper. The maximum vertical displacement of point B2 during single-train traffic is 0.9692 mm, and the maximum vertical displacement of point B2 during single-train traffic is 1.4484 mm. The response value of this paper is greater than the response value of the above research, which may be because the train speed set in this paper is twice that of the reference, and the diameter of the tunnel is greater. The above study only focuses on the vertical displacement of the double-track tunnel with the middle partition wall, while we make a full comparison of the dynamic response of the double-track tunnel with and without the middle partition wall, and analyze the dynamic response of the middle partition wall structure itself.

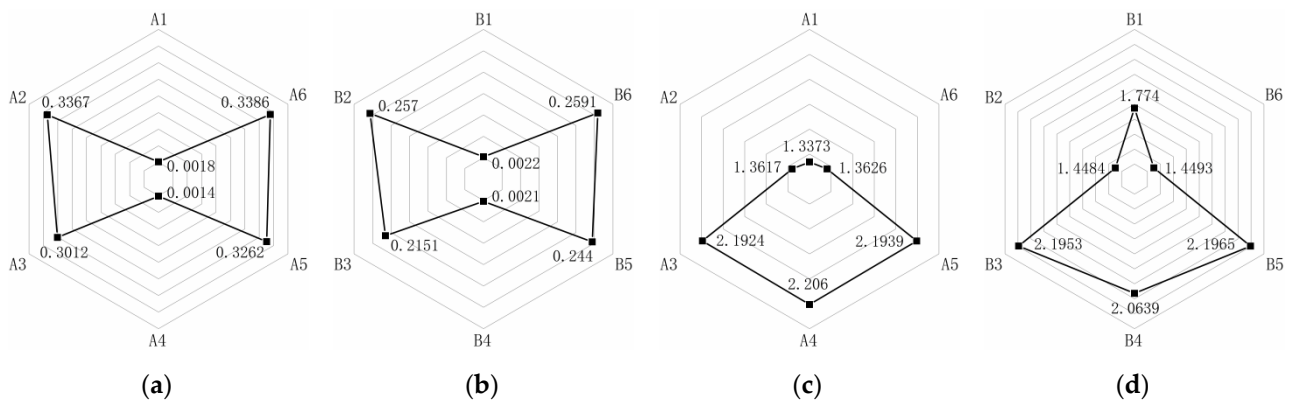


Figure 12. PPD (mm) during double-train traffic: (a) PPHD of double-track tunnel; (b) PPHD of double-track tunnel with middle partition wall; (c) PPVD of double-track tunnel; (d) PPVD of double-track tunnel with middle partition wall; A1-A6 and B1-B6 here correspond to that of A1-A6 and B1-B6 in Figure 9.

It can be seen from Figure 13a that the horizontal displacement response of C3 in the middle of the middle partition wall is the strongest during single-train or double-train traffic, and C4 is similar to C3. The PPHD of C3 is 0.1907 mm during double-train traffic, while the PPHD of C3 is 1.6492 mm during single-train traffic, which is about 8.65 times that of double-train traffic, which may be because most of the PPHD cancel each other out during double-train traffic, resulting in a substantial weakening of the horizontal displacement response. It can be seen from Figure 13b that since the bottom of the middle partition wall is closest to the point where the train vibration load is applied, the vertical displacement response of C5 at the bottom of the partition middle wall is the strongest during single-train or double-train traffic. The PPVD of the C5 is 1.7041 mm during single-train traffic, while the PPVD of the C5 is 3.3560 mm during double-train traffic, which is doubled, and the same is true for the rest of the measuring points. The train vibration load is applied to the track tread in the form of a vertical excitation load, so the vertical displacement response of double-train traffic increases exponentially. Figure 14a,b shows the displacement response diagrams of the measuring points with the strongest horizontal and vertical displacement responses, respectively. It can be seen that the displacement responses of the measuring points are the same as the train vibration load time–history curve, and both show a certain periodicity.

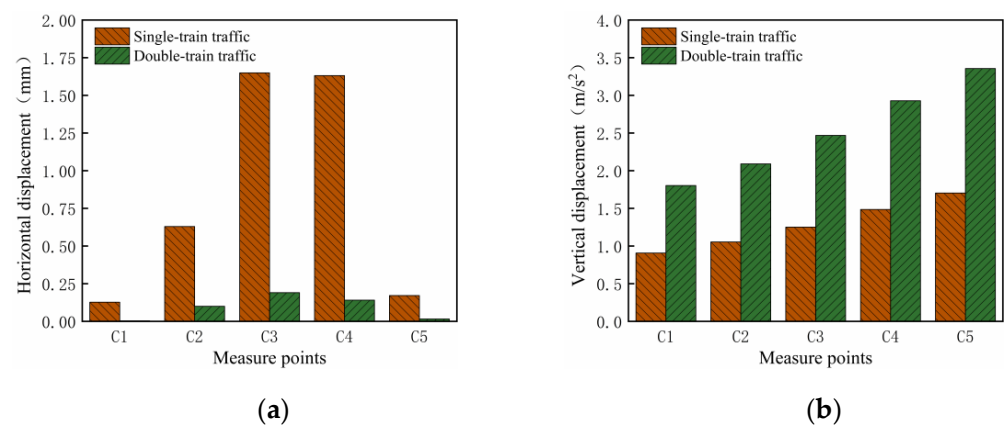


Figure 13. PPD of measuring point: (a) PPHD; (b) PPVD.

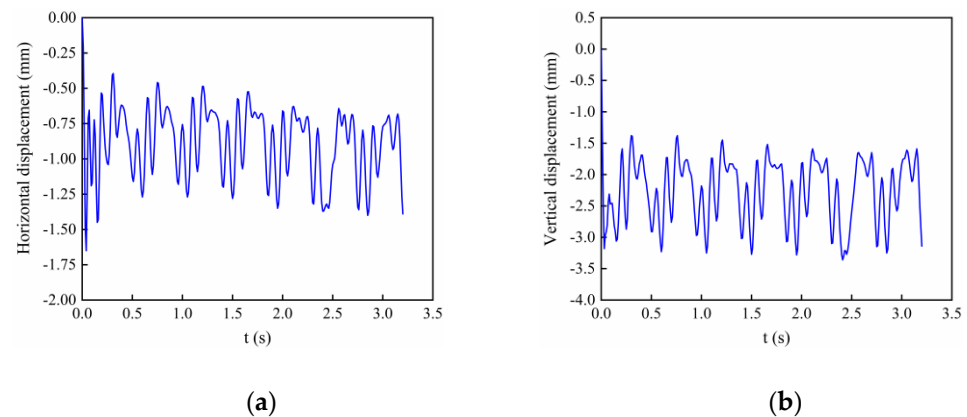


Figure 14. Displacement response of middle partition wall measuring point: (a) horizontal displacement response of C3 during single-train traffic; (b) vertical displacement response of C5 during double-train traffic.

4.2. Acceleration Response Analysis

It can be seen from Figure 15 that, similar to the displacement response law, when $t = 2.45$ s, the addition of the partition wall reduces the maximum acceleration response value of the tunnel from 18.51 m/s^2 to 16.62 m/s^2 , and greatly weakens the acceleration response of zone C, but the acceleration response in zone A is slightly enhanced, while zone B has no significant change.

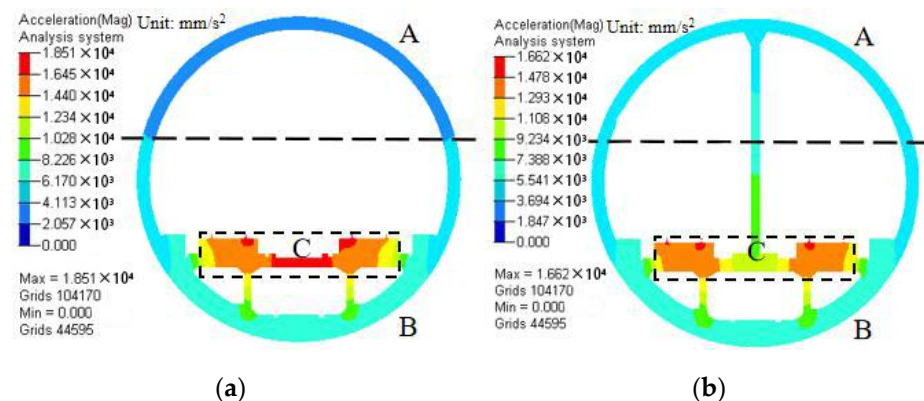


Figure 15. $t = 2.45$ s, tunnel acceleration response during double-train traffic: (a) double-track tunnel; (b) double-track tunnel with middle partition wall; zone A is the upper half of the tunnel, zone B is the lower half of the tunnel, zone C is the track bed and surrounding connections.

During single-train traffic, the graph outlines in (a) and (b) in Figure 16 are similar, except A2 is 29.0% higher than B2, and the *PPHA* of all measuring points of the double-track tunnel is slightly larger than that of the middle partition wall double-track tunnel. The graph outlines in (c) and (d) in Figure 16 are similar; the *PPVA* of B2 and B6 are slightly larger than those of A2 and A6, while the *PPVA* of the remaining four measuring points of the double-track tunnel are slightly larger than those of the middle partition wall double-track tunnel. In general, during single-train traffic, the acceleration response of one side of the train is stronger than the other. The horizontal acceleration response value of all measuring points in the double-track tunnel is larger than that of the middle partition wall double-track tunnel, while the vertical acceleration response value of the two is closer. In other words, their acceleration responses are similar during single-train traffic.

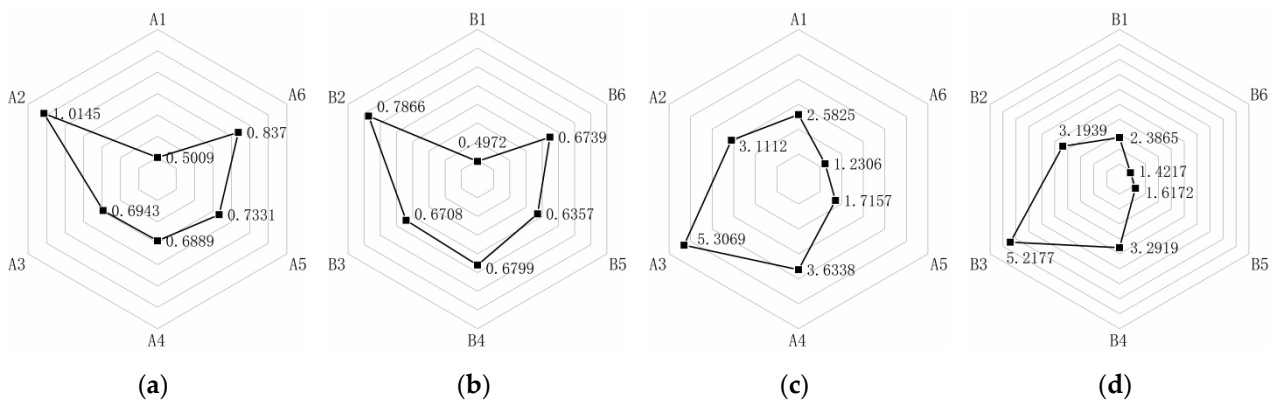


Figure 16. PPA (m/s^2) during single-train traffic: (a) PPHA of double-track tunnel; (b) PPHA of double-track tunnel with middle partition wall; (c) PPVA of double-track tunnel; (d) PPVA of double-track tunnel with middle partition wall; A1–A6 and B1–B6 here correspond to that of A1–A6 and B1–B6 in Figure 9.

Comparing (a) and (b) in Figure 17 during double-train traffic, the horizontal displacement response is similar to that of single-train traffic; the contours are the same, in the shape of a bow; the left and right sides are symmetrical; and the PPHA at the axis of symmetry is the smallest, with the PPHA of A2, A3, A5, and A6 being about 45% higher than that of the corresponding measuring points of the double-track tunnel with the middle partition wall. The graph outlines of (c) and (d) in Figure 17 are similar, and are similar to the vertical acceleration response during single-train traffic. The PPVA is slightly larger than that of the middle partition wall double-track tunnel. In general, during double-train traffic, the displacement responses of the double-track tunnel and the double-track tunnel with the middle partition wall are distributed symmetrically, and the horizontal acceleration response of the double-track tunnel is larger than that of the double-track tunnel with the middle partition wall. The train vibration load is applied in the form of vertical excitation load, and the application of the middle partition wall makes the upper and lower parts of the tunnel lining have more connections, which transfers part of the vertical displacement response of the lower part to the upper part.

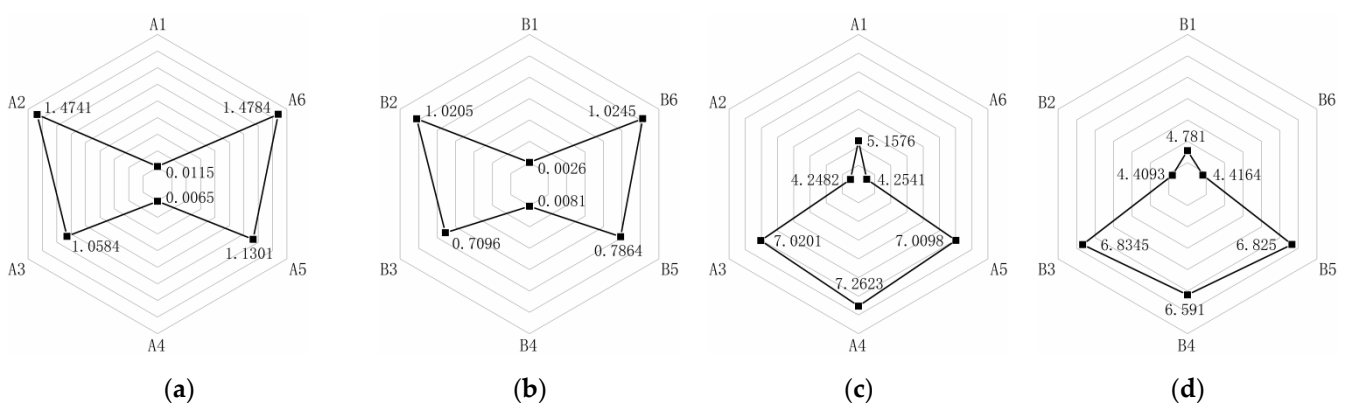


Figure 17. PPA (m/s^2) during double-train traffic: (a) PPHA of double-track tunnel; (b) PPHA of double-track tunnel with middle partition wall; (c) PPVA of double-track tunnel; (d) PPVA of double-track tunnel with middle partition wall; A1–A6 and B1–B6 here correspond to that of A1–A6 and B1–B6 in Figure 9.

From Figure 18a, it can be seen that the horizontal acceleration response of C3 in the middle of the middle partition wall is the strongest during single-train or double-train traffic, and C4 is similar to C3. During double-train traffic, the PPHA of C3 is 6.1293 m/s^2 , while during single-train traffic, the PPHA of C3 is 0.2151 m/s^2 , which is about 28.5 times

that of double-train traffic. This may be due to the fact that most *PPHA* cancel each other out during double-train traffic, resulting in a substantial weakening of the horizontal acceleration response. It can be seen from Figure 18b that since the bottom of the partition wall is closest to the point where the train vibration load is applied, the vertical acceleration response at the bottom of the middle partition wall C5 is the strongest. During single-train traffic, the *PPVA* of the C5 is 4.6473 m/s^2 , while the *PPVA* of the C5 is 9.1740 m/s^2 during double-train traffic, which is almost doubled, and the same is true for the rest of the measuring points. This is because the train vibration load is applied to the track tread in the form of a vertical excitation load, so the vertical acceleration response during double-track traffic increases exponentially. Figure 19a,b shows the acceleration response diagrams of the measuring points with the strongest horizontal and vertical acceleration responses, respectively, and the acceleration responses of the measuring points also show a certain periodicity.

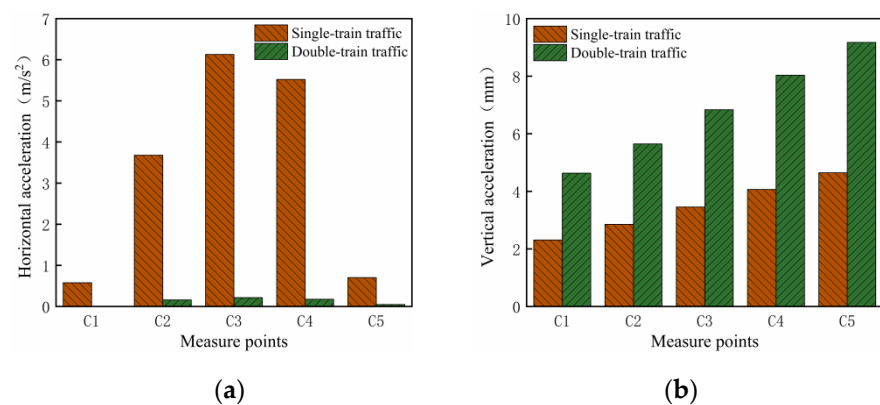


Figure 18. PPA of measuring point: (a) PPHA; (b) PPVA.

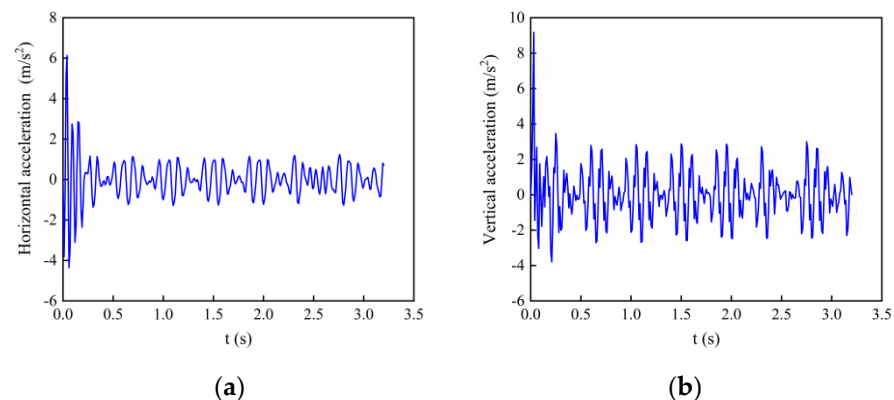


Figure 19. Acceleration response of middle partition wall measuring point: (a) horizontal acceleration response of C3 during single-train traffic; (b) vertical acceleration response of C5 during double-train traffic.

5. Conclusions

Using the numerical simulation method, we established detailed double-track tunnel-soil models with and without a middle partition wall, and studied the influence of adding a middle partition wall on the dynamic response distribution of the double-track tunnel structure.

- (1) The addition of a middle partition wall in a double-track tunnel has brought significant changes to the dynamic response distribution of the tunnel structure. The dynamic response distribution of the double-track tunnel structure is more uniform. The maximum displacement response value of the tunnel decreases from 5.881 mm to 5.335 mm, and the maximum acceleration response value changes from 18.51 m/s^2 to

16.62 m/s². The vertical displacement and acceleration responses show an increasing trend, but the horizontal displacement and acceleration responses show a weakening trend. The addition of the partition wall connects zone A and zone C. The displacement response value of zone A increases from 1.0 mm to 1.5 mm, and the acceleration response value increases from 3.0 m/s² to 4.6 m/s². The displacement response value of zone C decreases from 5 mm to 3 mm, a decrease of about 40%. The acceleration response value of zone C decreases from 18 m/s² to 10 m/s², a decrease of about 45%. There is no significant change in zone B.

- (2) Compared with single-train traffic, the addition of the middle partition wall brings more obvious changes to the dynamic response of the double-track tunnel during double-train traffic. During double-train traffic after adding the middle partition wall, the horizontal displacement and horizontal acceleration response values of the double-track tunnel structure decrease by about 30% to 45%, the horizontal displacement of B2 decreases from 0.3386 mm to 0.2591 mm, and the horizontal acceleration decreases from 1.4784 m/s² to 1.0245 m/s². The vertical displacement response value of the connection between the middle partition wall and the lining increases from 1.337 mm to 1.774 mm, an increase of 32.7%, and the vertical acceleration of the lower half of the tunnel lining is partially transferred to the upper half.
- (3) Under the train vibration load, the dynamic response of the middle partition wall structure has certain rules. The horizontal displacement and acceleration response values of the middle of the middle partition wall are the largest, which are 1.6 mm and 6.0 m/s², and the vertical displacement and acceleration response values of the bottom of the middle partition wall are the largest, which are 3.3 mm and 9.0 m/s². The horizontal displacement and acceleration response values during double-train traffic are only 1/8 and 1/28 of those during single-train traffic, and the vertical displacement and acceleration response during single-train traffic are 1/2 of those during single-train traffic.
- (4) In this study, the influence of the middle partition wall on the dynamic response of the double-track tunnel was analyzed by establishing a two-dimensional finite element tunnel model, but it lacked the support of experimental data. In the future, field measurements or physical model tests will be considered, and a three-dimensional finite element model will be established to further study the tunnel dynamic response in time and space.

Author Contributions: Conceptualization, S.Y.; methodology, S.Y.; software, J.H.; formal analysis, P.X.; data curation, J.H.; writing—original draft preparation, J.H.; writing—review and editing, S.Y.; supervision, P.X.; project administration, P.X. All authors have read and agreed to the published version of the manuscript.

Funding: This research was funded by [the National Key Research and Development Program of China, the Natural Science Foundation of Hunan Province and the Leading Talents of Science and Technology in Hunan Province] grant number [2021YFB3703801-04, 2021JJ30853 and 2019RS3018] And The APC was funded by [2021YFB3703801-04, 2021JJ30853 and 2019RS3018].

Data Availability Statement: The data presented in this study are available on request from the corresponding author. The data are not publicly available because this research project has not been completed and formally accepted.

Acknowledgments: Thanks to funding for supporting this study. Thanks to Peng Zhang for correcting a lot of grammatical and formatting mistakes in the manuscript.

Conflicts of Interest: The authors declare no conflict of interest.

References

1. Yang, W.; Zhang, C.; Liu, D.; Tu, J.; Yan, Q.; Fang, Y.; He, C. The effect of cross-sectional shape on the dynamic response of tunnels under train induced vibration loads. *Tunn. Undergr. Space Technol.* **2019**, *90*, 231–238. [[CrossRef](#)]
2. Tsinidis, G.; Pitilakis, K.; Madabhushi, G. On the dynamic response of square tunnels in sand. *Eng. Struct.* **2016**, *125*, 419–437. [[CrossRef](#)]

3. Zhang, D.M.; Chen, S.; Wang, R.C.; Zhang, D.M.; Li, B.J. Behaviour of a large-diameter shield tunnel through multi-layered strata. *Tunn. Undergr. Space Technol.* **2021**, *116*, 104062. [[CrossRef](#)]
4. Li, L.; Shang, C.; Chu, K.; Zhou, Z.; Song, S.; Liu, Z.; Chen, Y. Large-scale geo-mechanical model tests for stability assessment of super-large cross-section tunnel. *Tunn. Undergr. Space Technol.* **2021**, *109*, 103756. [[CrossRef](#)]
5. Fan, Z.; Zhang, J.; Xu, H. Theoretical study of the dynamic response of a circular lined tunnel with an imperfect interface subjected to incident SV-waves. *Comput. Geotech.* **2019**, *110*, 308–318. [[CrossRef](#)]
6. Juan, H.; Limin, P.; Zude, D.; Mingfeng, L. Vibration response analysis of high-speed railway tunnel structure based on damage theory. *Mod. Tunn. Technol.* **2017**, *54*, 93–100.
7. Real, T.; Zamorano, C.; Ribes, F.; Real, J. Train-induced vibration prediction in tunnels using 2D and 3D FEM models in time domain. *Tunn. Undergr. Space Technol. Inc. Trenchless Technol. Res.* **2015**, *49*, 376–383. [[CrossRef](#)]
8. Luo, J.; Zhang, D.; Fang, Q.; Liu, D.; Xu, T. Mechanical responses of surrounding rock mass and tunnel linings in large-span triple-arch tunnel. *Tunn. Undergr. Space Technol.* **2021**, *113*, 103971. [[CrossRef](#)]
9. Gao, Y. *Vibration Response and Safety Evaluation of Trains in Large Diameter Shield Tunnel of Intercity Railway*; North China University of Water Resources and Electric Power: Zhengzhou, China, 2020.
10. Xiaoke, L.; Yu, G.; Haichao, L.; Kaishu, C.; Hui, W. Vibration Response Analysis of Large Diameter Shield Tunnel for Intercity Railway with Two-orbit Trains. *Sci. Technol. Eng.* **2021**, *21*, 6.
11. Bing, B.; Chunfeng, L. Elastoplastic dynamic responses of close parallel metro tunnels to vibration loading. *Rock Soil Mech.* **2009**, *30*, 6.
12. Junli, Z. Construction technology of partition wall in the southern section of Shanghai Rail Transit Line 11. *Tunn. Constr.* **2015**, *35*, 4.
13. Bingwei, Y.; Bocong, L. Research on Key Construction Technology of Middle Partition Wall Trolley in Large Section Tunnels in Subway Engineering. *Eng. Technol. research.* **2022**, *7*, 10.
14. Yongping, S. Construction technology of partition wall in large diameter tunnel of urban rail transit. *Undergr. Eng. Tunn.* **2014**, *1*, 5.
15. Shouwen, X. Practice of Partition Wall Construction Technology in Prefabricated Partition Tunnel in Rail Transit Interval. *China Stand.* **2017**, *2*, 1.
16. Bo, W. Construction technology of partition wall in large diameter subway tunnel. *Urban Road Bridges Flood Control.* **2014**, *5*, 5.
17. Liang, Z. Construction Technology of Partition Wall of $\Phi 11.36\text{m}$ Metro Tunnel. *Build. Constr.* **2012**, *34*, 3.
18. Kai, C.; Liu, Y.; Jie, C. Key Technologies of Partition Wall Construction in Single-Hole and Double-Line Subway Tunnels. In Proceedings of the 15th Annual Meeting of the Chinese Civil Engineering Society and the 17th Annual Meeting of the Tunnel and Underground Engineering Branch, Kunming, China, 9–12 October 2012.
19. Mingxiang, Y. Construction of partition wall in large diameter shield tunnel. *Build. Constr.* **2018**, *40*, 3.
20. Zhongjie, Z.; Guanlin, Y.; Xiang, T. Case Study on Influence of Separation Wall on Deformation of Large Cross-section Shield-bored Tunnel on No.16 Line of Shanghai Metro. *Tunn. Constr.* **2014**, *34*, 6.
21. Hu, B.; Jin, X.-L.; Zhan, C.-B.; Luo, C. Numerical simulation of the nonstop crossing of opposite subways in a single bore tunnel. *J. Vib. Shock.* **2015**, *34*, 8.
22. Li, L.; Zhang, B.Q.; Yang, X.L. Analysis of dynamic response of large cross-section tunnel under vibration load induced by high speed train. *Chin. J. Rock Mech. Eng.* **2016**, *24*, 4259–4265.
23. Xiangqiu, W.; Linde, Y.; Zhiguo, Z. Dynamic Response Analysis of Lining Structure for Tunnel under Vibration Loads of Train. *Chin. J. Rock Mech. Eng.* **2006**, *25*, 6.
24. Abuhajar, O.; El Naggar, H.; Newson, T. Experimental and numerical investigations of the effect of buried box culverts on earthquake excitation—ScienceDirect. *Soil Dyn. Earthq. Eng.* **2015**, *79*, 130–148. [[CrossRef](#)]
25. Maleska, T.; Beben, D.; Nowacka, J. Seismic vulnerability of a soil-steel composite tunnel-Norway Tolpinrud Railway Tunnel Case Study. *Tunn. Undergr. Space Technol.* **2021**, *110*, 103808. [[CrossRef](#)]
26. Katona, M.G. Seismic Design and Analysis of Buried Culverts and Structures. *J. Pipeline Syst. Eng. Pract.* **2010**, *1*, 111–119. [[CrossRef](#)]
27. Li, C. The Dynamic Response of Close Crisscross and Overlapping Tunnels under Subway Load. Doctoral Dissertation, Beijing Jiaotong University, Beijing, China, 2006.
28. Liying, M.A.; Maoqi, L.I.; Wei, W.; Yuanwen, C. FEM Analysis and Experimental Research of Vibration Compaction Based on Drucker-Prager Model. *J. Chongqing Jiaotong Univ. (Nat. Sci.)* **2019**, *38*, 6.
29. Li, S.; Chen, P.; Li, G. Statistical Damage Constitution Model of Cement-soil Based on Drucker-Prager Criterion. *Transp. Sci. Technol.* **2021**, *306*, 3.
30. Cai, X.; Yang, J. Structural Behaviour of FRP-confined Concrete by Drucker-Prager Model. *Struct. Eng.* **2018**, *34*, 9. [[CrossRef](#)]
31. Lysmer, J.; Kuhlemeyer, R.L. Finite Dynamic Model for Infinite Media. *J. Eng. Mech. Div.* **1969**, *95*, 859–878. [[CrossRef](#)]
32. Juan, H. *Study on the Vibration Response and Fatigue Life of High-Speed Railway Tunnels Based on Damage Theory*; Central South University: Changsha, China, 2009.
33. Lei, L.; Mengxi, Z.; Huiming, W. Influence of metro train loading calculation methods on dynamic response of shield tunnel. *J. Shanghai Jiao Tong Univ.* **2015**, *49*, 5.

34. Bo, L.; Ying, C. Dynamic Analysis on Subgrade of High Speed Railways in Geometric Irregular Condition. *J. China Railw. Soc.* **1999**, *21*, 5.
35. Bo, L.; Hong, L.; Changxin, S. Simulated Study on Vibration Load of High Speed Railway. *J. China Railw. Soc.* **2006**, *28*, 6.
36. Yue, Z.; Baohong, B. Numerical analysis of vibration response in High-speed Railway Tunnel. *J. Vib. Shock.* **2001**, *20*, 3.
37. Zude, D. Analysis of influence factors on dynamic response of high-speed railway tunnel under vibration load. *J. Railw. Sci. Eng.* **2011**, *8*, 6.
38. The Second Design Institute of Ministry of Railways. *Railway Engineering Design Technical Manual-Tunnel*; People's Railway Publishing House: Beijing, China, 1978.
39. Songjie, C. Analysis of Train Vibration Response in Shield Tunnel of Underwater High-Speed Railway in Soft Stratum. Doctoral Dissertation, Central South University, Changsha, China, 2010.
40. Zhao, C. Study on Dynamic Characteristics of Metro Train under Vibration Load. Doctoral Dissertation, Beijing University of Civil Engineering and Architecture, Beijing, China, 2020.
41. Tian, T.; Guoqing, L.; Faling, Q.; Jun, D. Analysis on acceleration response of tunnel lining under vibration load of train with speed of 300 km/h. *J. China Railw. Soc.* **2020**, *42*, 9.
42. Li, T.; Su, Q.; Kaewunruen, S. Influences of piles on the ground vibration considering the train-track-soil dynamic interactions. *Comput. Geotech.* **2020**, *120*, 103455. [[CrossRef](#)]